SAND2015-2367C

Proceedings of the ASME 2015 International Design Engineering Technical Conferences & Computers and Information in Engineering Conference
IDETC/CIE 2015
August 2-5, 2015, Boston, USA

DETC2015-46301

PREDICTION OF ISOLATED RESONANCE CURVES USING NONLINEAR NORMAL MODES

R.J. Kuether
Engineering Physics
University of Wisconsin-Madison, WI
Email: rkuether@wisc.edu

L. Renson
Aerospace and Mechanical Eng.
University of Liege, Belgium
Email: l.renson@ulg.ac.be

T. Detroux
Aerospace and Mechanical Eng.
University of Liege, Belgium
Email: tdetroux@ulg.ac.be

C. Grappasonni
Aerospace and Mechanical Eng.
University of Liege, Belgium
Email: chiara.grappasonni@ulg.ac.be

G. Kerschen
Aerospace and Mechanical Eng.
University of Liege, Belgium
Email: g.kerschen@ulg.ac.be

M.S. Allen
Engineering Physics
University of Wisconsin-Madison, WI
Email: msallen@engr.wisc.edu

ABSTRACT

Isolated resonance curves are separate from the main nonlinear forced-response branch, so they can easily be missed by a continuation algorithm and the resonant response might be underpredicted. The present work explores the connection between these isolated resonances and the nonlinear normal modes of the system and adapts an energy balance criterion to connect the two. This approach provides new insights into the occurrence of isolated resonances as well as a method to find an initial guess to compute the isolated resonance curve using numerical continuation.

The concepts are illustrated on a finite element model of a cantilever beam with a nonlinear spring at its tip. This system presents jumps in both frequency and amplitude in its response to a swept sinusoidal excitation. The jumps are found to be the result of a modal interaction that creates an isolated resonance curve that eventually merges with the main resonance branch as the excitation force increases. Excellent insight into the observed dynamics is provided with the NNM theory, which supports that NNMs can also be a useful tool for predicting isolated resonance curves and other behaviors in the damped, forced response.

1 INTRODUCTION

Nonlinearity is important in many structural dynamic applications that are of interest to engineers, for example in structures with bolted interfaces [1] or machinery with rubber isolation mounts. In other cases the baseline structure is linear, but its performance can be enhanced by adding or engineering certain types of nonlinearities [2, 3]. Nonlinear dynamics is a rich and complicated field and new analysis techniques have to be developed to provide insight into the behavior of the system.

Vibration modes form the foundation of our understanding of linear dynamic systems, and influence efforts related to testing, modeling, validating and controller design. Rosenberg [4] extended modal analysis to nonlinear systems in the 1960's, coining the phrase nonlinear normal mode (NNM). The area received new attention in the 1990's [5–7] and now it is clear that NNMs can be used to obtain a wealth of insight into the response of a nonlinear system [6, 8]. For example, NNMs have been used to explain internally resonant and non-resonant motions of structures [9, 19], to design a nonlinear vibration absorber (also called a nonlinear energy sink) [2], to create or validate a reduced order model for a system [10], and to explain

changes in the oscillation frequency and the deformation shape of the free and forced response of a structure [8].

In recent years important progress has been made in the numerical calculation of undamped [11–14] and damped NNMs [15, 16]. These new algorithms have been used to compute the nonlinear modes of a geometrically nonlinear finite element model of a component from a diesel exhaust system, a full-scale aircraft, a bladed disk from a turbine and a strongly nonlinear satellite in [12,17–19], respectively.

One fundamental property of undamped NNMs is the fact that they can be realized when a harmonic forcing function cancels the damping force in the damped system [20]. As a result, they form the backbone of the nonlinear forced response (NLFR) curves [7, 8, 24] and hence they approximate the oscillation frequency and deformation shape that are exhibited at resonance, when a structure is at the greatest risk of failure. The relationship between the NLFR and the NNM backbone is simple for mild nonlinearities, but most realistic systems exhibit complicated NNMs with many interactions between the various modes leading to internally resonant branches.

This work explores the relationships between these interacting NNMs and the forced response of the nonlinear system, especially for the case in which the forced response shows an isolated resonance curve (IRC). Specifically, we show that the interactions between NNMs are responsible for the IRCs in the forced response. We note that the paper [25] discusses the relationships between bifurcations of backbone curves and IRCs; it is therefore the ideal companion of the present study. These detached families of solutions are frequently not detected because they do not emerge naturally from the fundamental response when numerical continuation is used. They can lie outside or inside the main resonance curve [26, 27], with the former case typically being more important because one is likely to underestimate the response of the nonlinear system [28, 29].

The paper is organized as follows. Section 2 reviews the methodology used to compute the periodic motions of the undamped and damped form of the nonlinear equations of motion, along with a phase resonance condition extended to nonlinear systems. An adaptation of the energy balance procedure presented by Neild et al. [30, 31], which can be used to estimate the forcing amplitude required to isolate the NNM is also presented in Section 2, drawing a direct connection between the damped and undamped periodic solutions. The nonlinear modes of a linear cantilever beam with a cubic nonlinear spring attached at the beam tip are computed in Section 3 and the NLFR is presented in Section 4. An IRC is discovered near one of the modal interactions of the underlying undamped NNMs. Section 5 explores the effect of damping on the IRCs by tracking the fold bifurcations in the NLFR as the level of damping changes. The conclusions of the present study are presented in Section 6.

2 PERIODIC SOLUTIONS OF A NONLINEAR SYSTEM

2.1 Undamped System: Nonlinear Normal Modes

The N-degree-of-freedom (DOF) equations of motion (EOM) for a nonlinear finite element model generally can be written as

$$\mathbf{M}\ddot{\mathbf{x}} + \mathbf{C}\dot{\mathbf{x}} + \mathbf{K}\mathbf{x} + \mathbf{f}_{NL}(\mathbf{x}) = \mathbf{f}(t) \tag{1}$$

The $N \times N$ matrices $\mathbf{M}$, $\mathbf{C}$, and $\mathbf{K}$ respectively represent the linear mass, damping and stiffness matrices commonly used for linear models. The displacement, velocity and acceleration are represented with the $N \times 1$ vectors $\mathbf{x}$, $\dot{\mathbf{x}}$, and $\ddot{\mathbf{x}}$, and the external loads are applied through the $N \times 1$ force vector $\mathbf{f}(t)$. The $N \times 1$ nonlinear restoring force vector, $\mathbf{f}_{NL}(\mathbf{x})$, accounts for the nonlinearity in the physical system. In this work we only consider the case where the nonlinear restoring force depends on displacement.

The undamped NNM definition used in this work comes from the works of Lee [32] and Kerschen et al. [8]. They defined an NNM as *a not necessarily synchronous periodic motions of the conservative equations of motion.* By this definition, the periodic motions that occur when two or more modes interact are still considered NNMs since they relaxed the restriction of synchronous motion defined originally by Rosenberg [4].

A periodic solution satisfies the condition

$$\mathbf{z}(t+T) = \mathbf{z}(t), \quad \forall t \tag{2}$$

The state of the system $\mathbf{z} = [\mathbf{x}^{\mathrm{T}} \ \ \dot{\mathbf{x}}^{\mathrm{T}}]^{\mathrm{T}}$, where $(\cdot)^{\mathrm{T}}$ represents the transpose operator, relates to the displacement and velocity of the undamped form of Eq. (1). A variety of methods exist to find the periodic solutions (or NNMs) for the undamped EOM. In this work we employ the shooting technique [33] combined with numerical integration and a Newton-Raphson scheme to iteratively find the periodic solutions that satisfy Eq. (2). A shooting function $\mathbf{H}$ is defined as the difference between the initial state and the state of the system after some period of integration, T:

$$\mathbf{H}(\mathbf{z}_0, T) = \mathbf{z}(\mathbf{z}_0, T) - \mathbf{z}_0 = \mathbf{0}. \tag{3}$$

Given an initial state, $\mathbf{z}_0$, and a minimum oscillation period, T, that satisfy the periodicity condition in Eq. (3) to some numerical tolerance, the resulting periodic motion over that period is subsequently defined as the NNM.

When the shooting technique is combined with numerical continuation (as done in [12,14]), a continuous branch of NNMs is computed, showing the evolution of the periodic motions as the energy changes. Numerical continuation requires that a known solution exist in order to trace out a branch of solutions, making the linear normal modes at low energy an excellent starting point.

2.2 Damped System: Nonlinear Forced Response

The damped system includes the linear damping and external forces in the EOM, exactly as given in Eq. (1). In this work, the periodic motions refer to the steady state motion in response to a monoharmonic excitation force, which is defined as

$$\mathbf{f}(t) = \mathrm{Re}\left(\mathbf{F}e^{i\omega t}\right) \tag{4}$$

The complex amplitude vector $\mathbf{F}$ is arbitrarily applied at any of the system's DOF. The steady state response to the force in Eq. (4) at each forcing frequency, ω, is referred to as the nonlinear forced response (NLFR).

In this work we employ an algorithm that is similar to that used to find NNMs above, namely, shooting combined with numerical continuation in order to find the NLFR over a range of forcing frequencies. The shooting function is only slightly different from the one used to find the NNMs in Eq. (3), as

$$\mathbf{H}(\mathbf{z}_0, \omega, T) = \mathbf{z}(\mathbf{z}_0, \omega, T) - \mathbf{z}_0 = \mathbf{0} \tag{5}$$

This function evaluates the difference of the forced response at time T due to a forcing frequency ω and a set of initial conditions, $\mathbf{z}_0$. The shooting technique with numerical integration and a Newton-Raphson procedure is again combined with numerical continuation to find a continuous branch of solutions for a fixed forcing amplitude, $\mathbf{F}$. Unlike the linear case, the NLFR does not scale linearly with forcing amplitude, so a new NLFR branch must be computed for each amplitude of interest.

The NLFR reveals new phenomena that cannot be observed with linear theory, such as frequency-energy dependence, subharmonic and superharmonic resonances, coexisting solutions, and stable/unstable periodic motions. The objective of this work is to study IRCs, which cannot be arrived at by continuing the main NLFR branch.

2.3 Resonance of a Nonlinear System: Phase Quadrature

A damped system can be made to respond in a single NNM motion of its underlying conservative system if a multi-point, multi-harmonic excitation is applied to the system in Eq. (1) [20]. Specifically, this force is given as

$$\mathbf{f}(t) = \sum_{k=1}^{\infty} \mathrm{Re}\left(\mathbf{F}_k e^{ik\omega t}\right) \tag{6}$$

The fully populated $N \times 1$ vector $\mathbf{F}_k$ corresponds to the complex amplitude of the force for the k^{th} harmonic frequency. Using a complex Fourier series representation of the response and the nonlinear restoring force in the EOM (1), each harmonic can be balanced to give the following two relations

$$-k^2\omega^2\mathbf{M}\mathbf{X}_k + \mathbf{K}\mathbf{X}_k + \mathbf{F}_{NL,k} = 0 \tag{7}$$

$$ik\omega\mathbf{C}\mathbf{X}_k = \mathbf{F}_k \tag{8}$$

The $N \times 1$ vectors $\mathbf{X}_k$ and $\mathbf{F}_{NL,k}$ are the complex amplitudes for the k^{th} harmonic of the response and nonlinear restoring force, respectively.

These equations reveal an important relationship between the forced response and the NNMs of the system. That is, if all harmonics of the force exactly cancel out the harmonics of the damping forces given by Eq. (8), then the periodic response will exactly satisfy the undamped EOM, as shown by Eq. (7), which by definition is an NNM. Equation (8) also shows there is a 90 degrees phase difference between each harmonic of the displacement and the force harmonics. This phase lag quadrature condition can be used to indicate when an NNM motion has been isolated from the NLFR.

Of course, in practice it is unlikely that the forcing of interest will exactly cancel damping as outlined above, because this requires that the force be distributed in space and that it be comprised of many harmonics. A few studies [20–23,35] have shown that an accurate approximation to the NNM can be obtained by a much simpler force that excites resonance. For example, Peeters et al. [20,21] explored whether a single-point, monoharmonic excitation could approximately isolate an NNM, and found good results in simulations and experiment with a lightly damped beam. In their efforts it was helpful to define a multi-harmonic mode indicator function (MIF) which indicates when the 90 degrees phase lag condition has been obtained. When a single-point sinusoidal force is applied to the nonlinear structure, which is the case considered herein, the MIF is defined as follows

$$\Delta_1 = \frac{\mathrm{Re}(\mathbf{X}_1)^* \mathrm{Re}(\mathbf{X}_1)}{\mathbf{X}_1^* \mathbf{X}_1} \tag{9}$$

where the operator $(\cdot)^*$ represents the complex conjugate transpose. Using the complex amplitude of the fundamental harmonic, $\mathbf{X}_1$, of the computed NLFR, the MIF in Eq. (9) indicates that resonance occurs when Δ_1 is equal to one.

2.4 Force Required to Obtain NNM Motion

The relationship between backbone curves and the forced response was also studied using an energy balancing technique in [30,31]. Based on the second-order normal form theory, the analytical developments hold for weakly nonlinear regimes of motion. This technique is slightly revisited herein by employing a numerical viewpoint, which allows one to consider more strongly nonlinear regimes.

Let us first consider a linear system. As shown in [36], if the system is oscillating in a linear normal mode denoted as $\mathbf{x}(t)$, then the damping forces instantaneously exert a distributed force $\mathbf{C}\dot{\mathbf{x}}(\mathbf{t})$ and the power dissipated at any instant is

$$P_{diss} = \dot{\mathbf{x}}(t)^{\mathrm{T}} \mathbf{C} \dot{\mathbf{x}}(\mathbf{t}) \tag{10}$$

and the total energy dissipated over one cycle is

$$E_{diss/cyc} = \int_0^T P_{diss}\, dt \tag{11}$$

Similarly, an arbitrary forcing function $\mathbf{f}(t)$ inputs energy into the system as

$$E_{in/cyc} = \int_0^T \dot{\mathbf{x}}(t)^{\mathrm{T}} \mathbf{f}(t)\, dt \tag{12}$$

At resonance, the energy dissipated by the damping forces must match the total energy input to the system over the period T. The balance is enforced by setting $E_{diss/cyc} = E_{in/cyc}$ [36]. For a single-point, monoharmonic force with complex amplitude $A + i0$, the scaling on A can be computed by satisfying

$$A \int_0^T \dot{\mathbf{x}}(t)^{\mathrm{T}} \left(\mathbf{e}_n e^{i\omega t}\right) dt = \int_0^T \dot{\mathbf{x}}(t)^{\mathrm{T}} \mathbf{C} \dot{\mathbf{x}}(\mathbf{t})\, dt \tag{13}$$

where $\mathbf{e}_n$ is a vector of zeros with a value of one at the location n, which is the point at which the force is applied. This energy balance criterion is a useful result, because it enables the practitioner to formally establish the direct link from the computed linear normal modes, i.e., the periodic motions of the undamped, unforced system, to the resonant response of the damped forced system.

The energy balance, $E_{diss/cyc} = E_{in/cyc}$, also holds for nonlinear systems. So, if both the NNMs $\mathbf{x}(t)$ and the damping $\mathbf{C}$ in the system are known, Eq. (13) can be readily used to estimate the forcing amplitude A that would excite the system at resonance with associated motion $\mathbf{x}(t)$. While it is common practice to excite a system using a monoharmonic force, one should note that higher harmonics might be necessary to achieve a reasonable approximation to the NNM motion, especially near internal resonances, so any calculations based on Eq. (13) should be regarded as approximate.

As in [30, 31], the energy balance criterion will prove useful for computing the forced resonant response in correspondence to the backbone curve. Sections 4 and 5 will show that it can also be used in conjunction with the NNM to find the forcing amplitude at which IRCs are created and to compute the corresponding forced response.

3 NUMERICAL CASE STUDY: NNMS OF A CANTILEVER BEAM

In the present and next sections, a model of a cantilevered beam with a cubic nonlinear spring attached at the beam tip is used to investigate the connection between undamped NNMs and the damped NLFR.

A schematic of the FEA model is shown in Fig. 1, which is similar to the one studied in [14]. A lumped mass of 0.5 kg was added $a = 0.31$ m from the fixed end. The addition of the mass lowered the second natural frequency most, while having a minimal effect on the first mode. This shifted the location of the 3:1 modal interaction with NNM 2 on the first NNM branch (as seen later in Fig. 2(a)). A linear finite element model of the planar beam was created in Abaqus using 20 B31 Euler-Bernoulli beam elements and imported in Matlab, giving a total of 60 DOFs, where each node had x and y displacement, and z rotation. The beam was 0.7 m in length, with a width and thickness of 0.014 m, and was constructed of structural steel with a Young's modulus of 205 GPa and a density of 7800 kg/m^3. The cubic nonlinear spring had a coefficient of $K_{NL} = 6 \times 10^9 N/m^3$, and was attached at the beam tip affecting only the transverse direction.

The first NNM of the cantilever beam was computed using the shooting and pseudo-arclength continuation algorithm, and the frequency-energy plot (FEP) is shown in Fig. 2(a), where the black line represents the stable periodic solutions and the red dots are unstable. As the response amplitude of the nonlinear mode increased, the continuation algorithm traced the family of periodic orbits forming a continuous branch of solutions. The FEP has two dis-

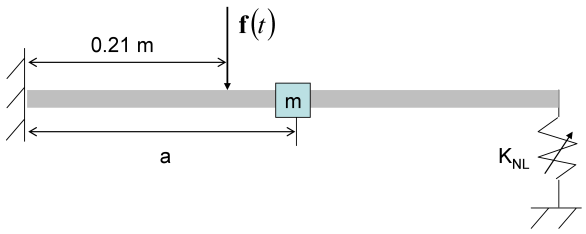

FIGURE 1: Schematic of a cantilever beam with a cubic nonlinear spring attached to the beam tip and a modifying lumped mass.

tinct features, namely a backbone, and tongues that emanate from the backbone. The backbone shows an increase in fundamental frequency as the energy in the periodic solutions increase revealing that the nonlinear spring has a stiffening effect on this mode. The tongues that emerged from the backbone are referred as modal interactions, or internal resonances, and occur when two or more NNMs interact.

The dashed, colored lines in Fig. 2(a) represent the frequency-energy behavior of the higher order NNMs after dividing the frequency by various integers. By shifting these NNMs down the frequency axis, it was possible to observe the location where the backbones of higher modes intersect with the NNM 1 backbone and cause a modal interaction to occur. Considering the modal interaction at approximately 37 Hz, which has the appearance of the Greek letter α and will hereafter be referred to as an α-tongue, the 1/3rd frequency branch of the NNM 2 branch intersects the backbone of NNM 1. This causes NNM 1 to bifurcate and create a 3:1 internal resonance tongue that has solutions where NNM 1 and 2 interact. The other three modal interactions along NNM 1 were a 9:1 interaction with NNM 3 near 44 Hz, a 15:1 interaction with NNM 4 near 47 Hz, and a 13:1 interaction with NNM 4 near 54 Hz.

Once the NNMs have been computed, Eq. (13) was used to estimate the monoharmonic driving force required to excite the NNM motion. A mass and stiffness proportional damping model was used, defining the damping matrix as $\mathbf{C} = a\mathbf{K} + b\mathbf{M}$ with $a = -0.0391$ and $b = 1.4710^{-4}$. These parameters were chosen such that the damping ratios of the first and second linear modes were 1% and 5%, respectively. The computed force amplitude and the corresponding frequency are displayed for the first NNM in Fig. 2(b). Interestingly, the force does not increase monotonically. For example, a force of 22.6 N could achieve resonance at about 37.5 Hz, 45.8 Hz and 47.4 Hz as shown with the circular markers. This has important implications for the forced response, as will be discussed in the next section.

4 NUMERICAL CASE STUDY: NLFR OF A CANTILEVER BEAM

4.1 Response to Sine Sweep Excitation

Some unexpected behavior occurred with the damped beam, using the same damping model described in the previous section, when a single-point force was applied 0.21 m from the fixed end in the transverse direction. A set of numerically computed sine sweeps are shown in Fig. 3, which plots the displacement of the beam tip for different force amplitudes, namely A = 11.3 N, 22.6 N, 26.7 N, 32.5 N, 35.6 N, and 45.2 N, with a sweep rate of 0.5 Hz/s. For reference, the response of the linear model at a force amplitude of A = 4.45 N was computed (black line), and resulted in the largest tip displacement (even though the force amplitude was the lowest), with a resonance at the linear natural frequency. The nonlinear spring caused the tip to displace at a significantly lower amplitude, and shifted the resonant frequency depending on the force amplitude. The nonlinear sweep at the force amplitude A = 11.3 N (red line) showed that resonance occurred near 37 Hz, resulting in a sudden jump, the so-called jump phenomenon, to a lower response amplitude as the frequency continued to sweep upwards. When the force amplitude doubled (green line, A = 22.6 N), the resonant frequency occurred near 39 Hz. However, doubling the force amplitude once more (cyan line, A = 45.2 N) caused a dramatic shift in resonant frequency and tip displacement. Now the response dropped off around 57 Hz, indicating that the increased force amplitude from 22.6 N to 45.2 N shifted the resonance nearly 18 Hz. Considering the amplitudes A = 32.5 N and 35.6 N (yellow and magenta lines) shows that the dramatic shift in resonant frequency occurred in this range of forcing amplitudes. Summarizing, Figure 3 depicts that *both a jump in amplitude (the well-known jump phenomenon) and a jump in frequency may exist for nonlinear systems.* We could not find other occurrences of simultaneous jumps in amplitude and frequency in the mechanical engineering literature.

Another dynamical phenomenon, which only appeared for A = 35.6 N and 45.2 N, is the modulation of the signal's envelope in the range of 40-45 Hz. It was further examined by monitoring bifurcations [37] along the NLFR (not shown here for brevity) [38]. Around 40 Hz, a Neimark-Sacker bifurcation changes the stability of the NLFR and generates a new branch of quasiperiodic oscillations. As a result, a stable torus attracts the dynamics and is responsible for the observed envelope modulation. Around 45 Hz, a second Neimark-Sacker bifurcation transforms the quasiperiodic motion back into stable periodic motion.

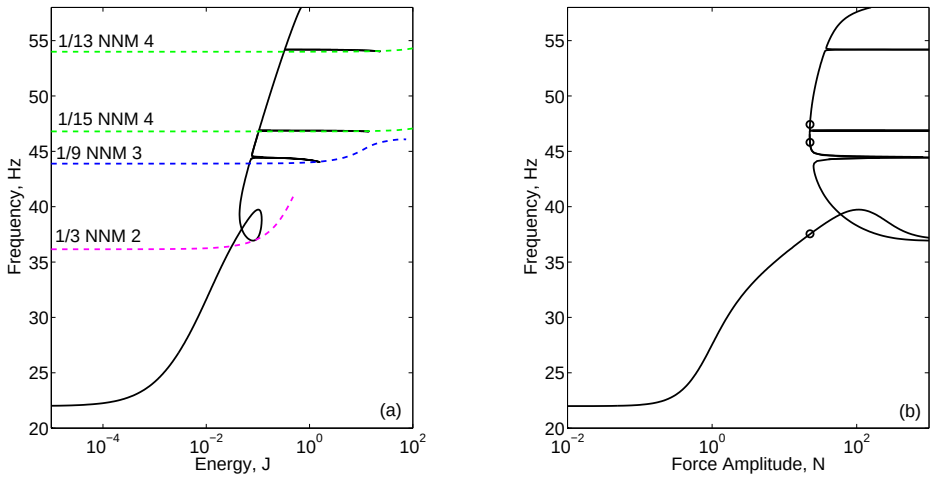

FIGURE 2: NONLINEAR BEAM. (a) FIRST NNM WITH VIEW OF THE CROSSING OF HIGHER ORDER NNMS IN DASHED LINES AT FRACTIONS OF THEIR FUNDAMENTAL FREQUENCY; (b) ESTIMATE OF FORCE AMPLITUDE REQUIRED TO OBTAIN THE MOTION GIVEN AT EACH POINT ON NNM 1, AS PREDICTED BY EQ. (13). CIRCULAR MARKERS INDICATE ACHIEVABLE RESONANCE FREQUENCIES FOR A FORCE OF 22.6 N.

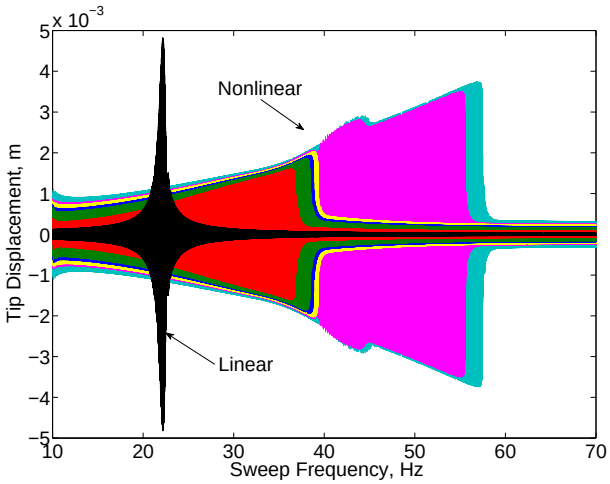

FIGURE 3: NUMERICAL SINE SWEEPS AT A RATE OF 0.5 HZ/S WHERE THE DISPLACEMENT OF THE BEAM TIP IS PLOTTED FOR FORCE AMPLITUDES OF (RED) 11.3 N, (GREEN) 22.6 N, (BLUE) 26.7 N, (YELLOW) 32.5 N, (MAGENTA) 35.6 N AND (CYAN) 45.2 N.

4.2 Response to Stepped Sine Excitation

An explanation for the jump in frequency of Fig. 3 was sought by computing the NLFR through a range of frequencies that spanned the first NNM. A single-point, monoharmonic force with arbitrary complex amplitude $A+i0$ was applied to the beam at the same location as the sweeps. The FEPs of the forced response at four different forcing amplitudes ($A = 0.445$ N, 0.890 N, 2.22 N and 4.45 N) are shown in the left plot of Fig. 4, where the energy on the horizontal axis represents the maximum energy of each steady-state solution in the NLFR, and the vertical axis represents the forcing frequency. The NNM was superposed on the plot to show how the forced response wraps around the NNM, acting as the backbone to the NLFR.

As the forcing frequency increased from 20 Hz, a fold bifurcation occurred in the NLFR and turned back around the backbone of the NNM. At this fold, the MIF from Eq. (9) in the right plot in Fig. 4 is approximately equal to 1 indicating that the NLFR approximately excited the NNM motion of the underlying undamped system.

Higher forcing amplitudes ($A = 11.3$ N, 22.6 N, 26.7 N, 35.6 N, and 45.2 N) were considered in Fig. 5 in order to examine the response near the α-tongue on NNM 1 and to match some of the amplitudes used in the sine sweep results. For $A = 11.3$ N in Fig. 5(a), the NLFR again wrapped around the backbone of the first NNM, as previously observed in Fig. 4. When the force amplitude doubled ($A = 22.6$ N in Fig. 5(b)), the resonance on the main NLFR branch occurred at 38.1 Hz and approached the 3:1 modal interaction on NNM 1. Initially, the green curve on the left is all that was computed by the continuation algorithm,

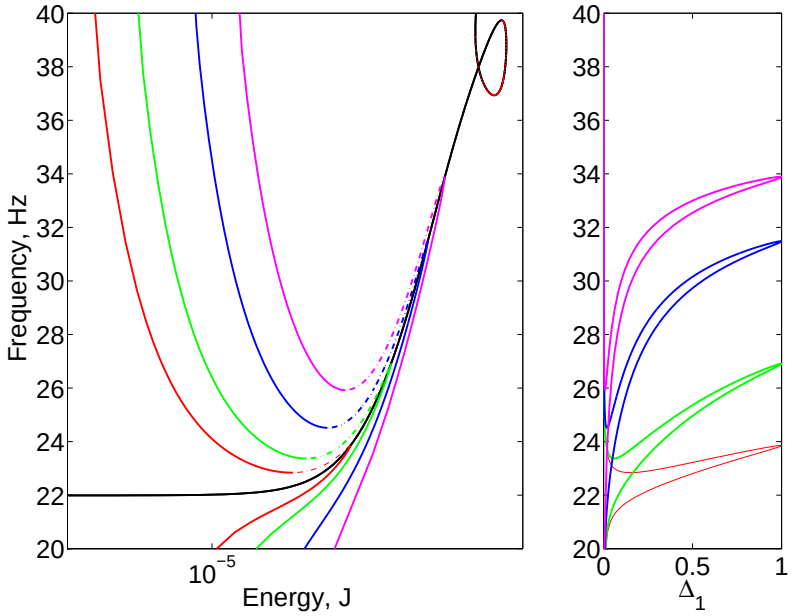

FIGURE 4: (LEFT) NONLINEAR FORCED RESPONSE CURVES AT FREQUENCIES NEAR THE FIRST NNM WHERE (SOLID) ARE STABLE PERIODIC MOTIONS AND (DASH DOT) ARE UNSTABLE PERIODIC MOTIONS. (RIGHT) MODE INDICATOR FUNCTION OF THE FORCED RESPONSE. THE FORCE AMPLITUDES FOR EACH CURVE ARE (RED) 0.445 N, (GREEN) 0.890 N, (BLUE) 2.22 N, AND (MAGENTA) 4.45 N.

since it started at low frequency and followed the curve upwards. However, the force estimated in Fig. 2(b) suggested that resonance might be excited at multiple points on the NNM using the same force. Specifically, this figure highlighted that a force of 22.6 N could achieve resonance at about 37.5 Hz, 45.8 Hz and 47.4 Hz. So the two latter points were used to initiate the NLFR algorithm and obtain the branch between 43 and 48 Hz in Fig. 5(b). This additional branch is referred to as an isolated resonance curve, or IRC. The response on this IRC is much larger than on the main branch so one would significantly underestimate the response if it was not found. By examining the NNMs and employing the energy balance criterion introduced in Sec. 2.4 we have avoided dramatically under-predicting the resonant response at this forcing amplitude. These new solutions still wrapped around the backbone of NNM 1 and corresponded to the NNM at two different frequencies, 43.9 Hz and 48.5 Hz, as indicated by the MIF. These frequencies are in relatively close agreement with the frequencies predicted using the energy balance criterion, 45.8 Hz and 47.4 Hz.

The forcing amplitude was slightly increased in Fig. 5(c) ($A = 26.7$ N), and the resonant frequency on the main branch did not shift very much (from 38.1 Hz to 38.5 Hz). The fold bifurcation on the main NLFR branch still transpired prior to the modal interaction on NNM 1. Again the IRC persisted and became larger, increasing its frequency range from 41 Hz to 51 Hz. A stable portion of the IRC has however become unstable through the emergence of Neimark-Sacker bifurcations (not represented). The latter will persist at higher forcing levels and are responsible for the quasiperiodic oscillations discussed in Fig. 3.

Increasing the amplitude even more ($A = 35.6$ N in Fig. 5(d)) caused the main branch and the IRC to merge together, forming one continuous NLFR branch up to 55 Hz. The merging of these two branches offers an explanation as to why the jump in resonant frequency occurred during the sine sweep excitation in Fig. 3. The sine sweeps at $A = 22.6$ N, $A = 26.7$ N and $A = 32.5$ N fell off around 38 Hz, because the IRC was disconnected from the main branch, and there was no path for the response to follow to the higher frequency resonance. However, once the two NLFR branches merged together (A=35.6 N), the sine sweeps were able to stay along the high amplitude path up to resonance around 55 Hz.

For the highest forcing amplitude shown ($A = 45.2$ N in Fig. 5(e)), the resonant frequency shifted to 56.6 Hz. This smooth increase in the resonant frequency and displacement amplitude continued at higher forces as well. Moving from Fig. 5(d) to Fig. 5(e) also caused one resonance to be

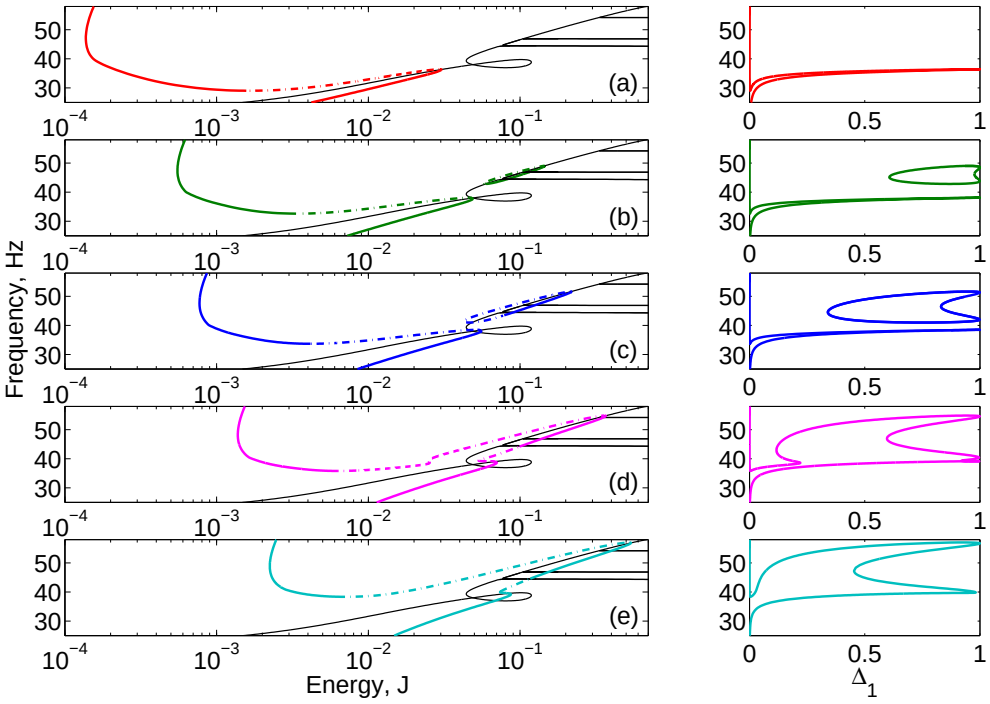

FIGURE 5: (LEFT) NONLINEAR FORCED RESPONSE CURVES AT FREQUENCIES NEAR THE FIRST NNM WHERE (SOLID) ARE STABLE PERIODIC MOTIONS AND (DASH DOT) ARE UNSTABLE PERIODIC MOTIONS. (RIGHT) MODE INDICATOR FUNCTION OF THE FORCED RESPONSE.THE FORCE AMPLITUDES FOR EACH CURVE (A - E) ARE (RED) 11.3 N, (GREEN) 22.6 N, (BLUE) 26.7 N, (MAGENTA) 35.6 N, AND (CYAN) 45.2 N, RESPECTIVELY.

eliminated, as indicated by the MIF.

The FEPs of the NNM and NLFR effectively condense the complicated dynamics of the nonlinear beam onto a two-dimensional plane. An additional comparison (not represented) between the time histories of the response for the NLFR and the corresponding NNM shows all were in good agreement. A slight phase shift was however observed for some solutions. This can be explained by the use of a mono-harmonic force input, whereas a multi-harmonic force would be needed to exactly isolate the NNM.

4.3 Energy Balance Criterion

For further validation of the energy balance criterion (13), Figure 6 superposes the responses of Figs. 4 and 5 where the MIF is equal to 1 onto Fig. 2(b). The cross markers, which represent the forced resonant response, are in close, though not exact, agreement with the predictions of the energy balance criterion.

Additional insight can be gained from this plot. For instance, one can guess from the leftmost point of the upper branch the amplitude and frequency at which the IRC is created, i.e., 22.3 N and 46.5 Hz. Considering that the IRC merges with the main branch around 35 N, the jump in frequency can be predicted by considering the point at 35 N on the upper branch at 53.8 Hz.

Finally, one important observation about the birth and the merging of the IRC was that they occurred when the main NLFR branch approached the 3:1 interaction between NNM 1 and NNM 2. Indeed, this interaction produced the non-monotonic increase in the forcing amplitude observed in Fig. 2(b), which was found to be the driving mechanism for IRC onset in Section 4.2. This demonstrates that interactions between NNMs are responsible for the IRCs in the forced response. It should be noted that this behavior was not found to occur with other modal interactions on the NNM branch whose tongues were sharper in the FEP. We also stress that the NNM definition relies on the underlying Hamiltonian system, whereas the NLFR is a result for the damped system. Damping also plays a role in the existence of IRCs, that is they may cease to exist if damping is large enough. This is illustrated in the next section.

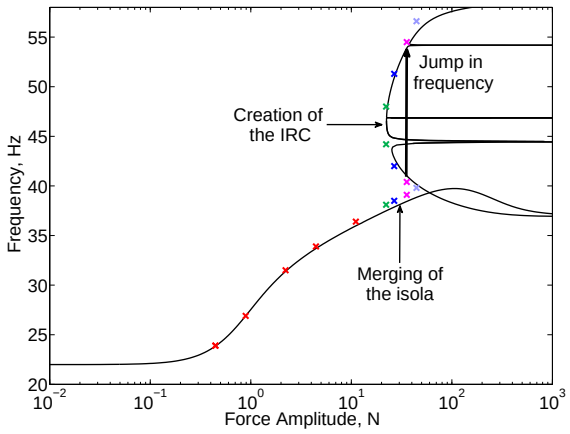

FIGURE 6: COMPARISON BETWEEN THE PREDICTIONS OF THE ENERGY BALANCE CRITERION (SOLID BLACK) AND THE FORCED RESONANCE WHERE THE MIF IS EQUAL TO ONE IN FIGS. 4 AND 5 (CROSS MARKERS).

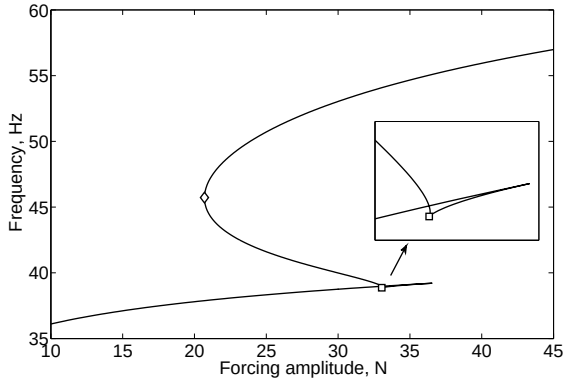

FIGURE 7: TRACKING OF FOLD BIFURCATIONS. PROJECTION OF THE BIFURCATION BRANCH ONTO THE (FORCING AMPLITUDE - ENERGY) PLANE. THE DIAMOND AND SQUARE MARKERS INDICATE THE APPARITION AND THE MERGING OF THE IRC, RESPECTIVELY.

5 INFLUENCE OF DAMPING

Bifurcation tracking in the codimension-2 space (frequency-forcing amplitude-energy) was performed in order analyze the evolution of the fold bifurcations for different forcing amplitudes. The procedure used in this section is based on the harmonic balance method described in [39], which approximates the periodic solutions with Fourier series (truncated to the first seven harmonics herein). Figure 7 gives a convenient projection of the bifurcation branch onto the frequency versus forcing amplitude plane. The turning point indicated with a diamond marker shows the frequency/forcing amplitude at which the fold bifurcations at the tips of the IRC were created. The corresponding values (45.7 Hz and 20.7 N) reflect the good predictive capability of the energy balance criterion (46.5 Hz and 22.3 N in Section 4.3). The square marker indicates when the IRC merges with the main resonance peak (33.1 N).

The fold bifurcation tracking analysis was again used to study the effect of structural damping on the observed IRCs. The damping matrix introduced in Section 4 was perturbed by adding a scaling term, κ, such that $\mathbf{C} = \kappa\left(-0.0391\mathbf{K} + 1.47\,10^{-4}\mathbf{M}\right)$. Several bifurcation branches are given in Fig. 8 for different values of κ, namely 1, 1.5, 1.8 and 1.9. The IRC was robust against damping since it was still visible for higher levels of damping ($\kappa > 1$), however, increasing κ caused the IRC to appear later in forcing amplitude, and shorten the range where it existed. For the largest damping case studied, for $\kappa = 1.9$, the IRC was no longer present. This analysis shows that a sufficiently large value of structural damping can destroy the IRCs.

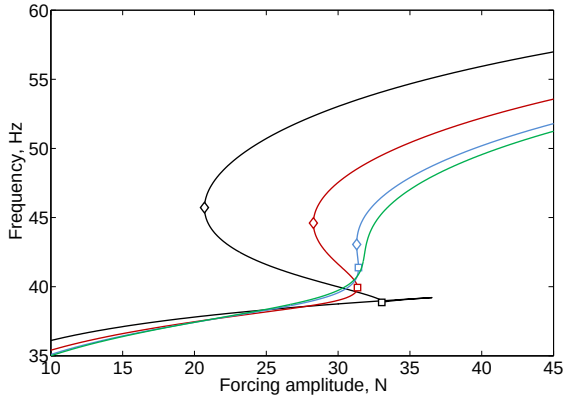

FIGURE 8: INFLUENCE OF DAMPING ON THE BIFURCATION BRANCHES. THE BLACK, RED, BLUE AND GREEN LINES DEPICT THE BRANCHES OF THE SYSTEM WITH $\kappa = 1$, 1.5, 1.8 AND 1.9, RESPECTIVELY. THE DIAMOND AND SQUARE MARKERS INDICATE THE APPARITION AND THE MERGING OF THE IRC, RESPECTIVELY.

6 CONCLUSIONS

This paper demonstrates the intimate connection that exists between nonlinear normal modes (NNMs), i.e., the

periodic motions of the undamped, unforced system, and the forced response of the damped system. To bridge the gap between these two types of response, the energy balance criterion was adapted so it could be used with the results of the numerical computations in order to estimate the resonant response to harmonic forcing from the NNMs and the damping matrix. This criterion strengthens the link that exists between NNMs and the resonant responses of the damped, forced system.

We have also shown that interactions between NNMs with non-necessarily commensurate linear frequencies are responsible for the isolated resonance curves (IRCs) in the forced response. IRCs, which might easily be missed during numerical continuation or experimental testing, have important practical consequences. The associated response can be much larger than on the main branch, and, when they connect to the main resonance branch, they may lead to a dramatic jump in frequency. To the best of our knowledge, this is the first time that this jump in frequency is observed in the mechanical engineering literature.

Finally, these developments extend the usefulness of the NNM concept to the interpretation of the complex dynamics exhibited by harmonically forced nonlinear systems.

ACKNOWLEDGMENT

The author RJ Kuether would like to acknowledge the funding for this part of this research from the National Physical Science Consortium (NPSC) Fellowship. The author L. Renson is Research Fellow (FRIA fellowship) of the *Fonds de la Recherche Scientifique - FNRS*, which is gratefully acknowledged. The authors T. Detroux, C. Grappasonni and G. Kerschen would like to acknowledge the financial support of the European Union (ERC Starting Grant NOVIB 307265).

References

[1] D.J. Segalman, D.L. Gregory, M.J. Starr, B.R. Resor, M.D. Jew, J.P. Lauffer, and N.M. Ames, *Handbook on Dynamics of Jointed Structures*, Sandia National Laboratories, Albuquerque, NM2009.

[2] O. Gendelman, Bifurcations of Nonlinear Normal Modes of Linear Oscillator with Strongly Nonlinear Damped Attachment, *Nonlinear Dynamics*, vol. 37, pp. 115-128, 2004.

[3] A.F. Vakakis, D.M. McFarland, L. Bergman, L.I. Manevitch, and O. Gendelman, Isolated Resonance Captures and Resonance Capture Cascades Leading to Single- or Multi-Mode Passive Energy Pumping in Damped Coupled Oscillators, *Journal of Vibration and Acoustics*, vol. 126, pp. 235-244, 2004.

[4] R. M. Rosenberg, Normal modes of Nonlinear Dual-Mode Systems, *Journal of Applied Mechanics*, vol. 27, pp. 263-268, 1960.

[5] S.W. Shaw, and C. Pierre, Normal Modes for Non-Linear Vibratory Systems, *Journal of Sound and Vibration*, vol. 164, pp. 85-124, 1993.

[6] A.F. Vakakis, Non-linear Normal Modes (NNMs) and their Applications in Vibration Theory: an Overview, *Mechanical Systems and Signal Processing*, vol. 11, pp. 3-22, 1997.

[7] A.F. Vakakis, L.I. Manevitch, Y.V. Mikhlin, V.N. Pilipchuk, and A.A. Zevin, *Nonlinear Modes and Localization in Nonlinear Systems*, New York, Wiley, 1996.

[8] G. Kerschen, M. Peeters, J.C. Golinval, and A.F. Vakakis, Nonlinear Normal Modes. Part I. A useful framework for the structural dynamicist, *Mechanical Systems and Signal Processing*, vol. 23, pp. 170-94, 2009.

[9] W. Lacarbonara, R. Camillacci, Nonlinear Normal Modes of Structural Systems via Asymptotic Approach, *International Journal of Solids and Structures*, vol. 41, pp. 5565-5594, 2004.

[10] C. Touzé and M. Amabili, Nonlinear Normal Modes for Damped Geometrically Nonlinear Systems: Application to Reduced-Order Modelling of Harmonically Forced Structures, Journal of Sound and Vibration, vol. 298, pp. 958-981, 2006.

[11] R. Arquier, S. Bellizzi, R. Bouc, and B. Cochelin, Two Methods for the Computation of Nonlinear Modes of Vibrating Systems at Large Amplitudes, *Computers & Structures*, vol. 84, pp. 1565-1576, 2006.

[12] R.J. Kuether and M.S. Allen, A Numerical Approach to Directly Compute Nonlinear Normal Modes of Geometrically Nonlinear Finite Element Models, *Mechanical Systems and Signal Processing*, vol. 46, pp. 1-15, 2014.

[13] D. Laxalde and F. Thouverez, Complex Non-linear Modal Analysis for Mechanical Systems: Application to Turbomachinery Bladings with Friction Interfaces, *Journal of Sound and Vibration*, vol. 322, pp. 1009-1025, 2009.

[14] M. Peeters, R. Viguié, G. Sérandour, G. Kerschen, and J. C. Golinval, Nonlinear Normal Modes, Part II: Toward a Practical Computation using Numerical Continuation Techniques, *Mechanical Systems and Signal Processing*, vol. 23, pp. 195-216, 2009.

[15] E. Pesheck, C. Pierre, and S.W. Shaw, New Galerkin-based Approach for Accurate Non-linear Normal Modes through Invariant Manifolds, *Journal of Sound and Vibration*, vol. 249, pp. 971-993, 2002.

[16] L. Renson, G. Deliége, and G. Kerschen, An Effec-

tive Finite-Element-Based Method for the Computation of Nonlinear Normal Modes of Nonconservative Systems, *Meccanica*, vol. 49, pp. 1901-1916, 2014.

[17] G. Kerschen, M. Peeters, J.C. Golinval, and C. Stephan, Nonlinear Normal Modes of a Full-Scale Aircraft, *AIAA Journal of Aircraft*, vol. 50, pp. 1409-1419, 2013.

[18] M. Krack, L. Panning-von Scheidt, and J. Wallaschek, A Method for Nonlinear Modal Analysis and Synthesis: Application to Harmonically Forced and Self-Excited Mechanical Systems, *Journal of Sound and Vibration*, vol. 332, pp. 6798-6814, 2013.

[19] L. Renson, J.P. Noel, and G. Kerschen, Complex Dynamics of a Nonlinear Aerospace Structure: Numerical Continuation and Normal Modes, *Nonlinear Dynamics*, in press.

[20] M. Peeters, G. Kerschen, and J.C. Golinval, Dynamic Testing of Nonlinear Vibrating Structures using Nonlinear Normal Modes, *Journal of Sound and Vibration*, vol. 330, pp. 486-509, 2011.

[21] M. Peeters, G. Kerschen, and J. C. Golinval, Modal Testing of Nonlinear Vibrating Structures based on Nonlinear Normal Modes: Experimental Demonstration, *Mechanical Systems and Signal Processing*, vol. 25, pp. 1227-1247, 2011.

[22] D. Ehrhardt, R. Harris, and M. Allen, Numerical and Experimental Determination of Nonlinear Normal Modes of a Circular Perforated Plate, in *Topics in Modal Analysis I*, Volume 7, J. De Clerck, Ed., ed: Springer International Publishing, 2014, pp. 239-251.

[23] J.L. Zapico-Valle, M. Garcia-Diéguez, and R. Alonso-Camblor, Nonlinear Modal Identification of a Steel Frame, *Engineering Structures*, vol. 56, pp. 246-259, 2013.

[24] A. Cammarano, T.L. Hill, S.A. Neild, D.J. Wagg, Bifurcations of Backbone Curves for Systems of Coupled Nonlinear Two Mass Oscillator, *Nonlinear Dynamics*, vol. 77, 311-320.

[25] T.L. Hill, P.L. Green, A. Cammarano and S.A. Neild, Fast Bayesian Identification of Multi-mode Systems using Backbone Curves, *Journal of Sound and Vibration*, in preparation.

[26] G. Gatti, M.J. Brennan, and I. Kovacic, On the Interaction of the Responses at the Resonance Frequencies of a Nonlinear Two Degrees-of-freedom System, *Physica D: Nonlinear Phenomena*, vol. 239, pp. 591-599, 2010.

[27] G. Gatti and M.J. Brennan, On the Effects of System Parameters on the Response of a Harmonically Excited System Consisting of Weakly Coupled Nonlinear and Linear Oscillators, *Journal of Sound and Vibration*, vol. 330, pp. 4538-4550, 2011.

[28] N.A. Alexander and F. Schilder, Exploring the Performance of a Nonlinear Tuned Mass Damper, *Journal of Sound and Vibration*, vol. 319, pp. 445-462, 2009.

[29] C. Duan and R. Singh, Isolated Sub-Harmonic Resonance Branch in the Frequency Response of an Oscillator with Slight Asymmetry in the Clearance, *Journal of Sound and Vibration*, vol. 314, pp. 12-18, 2008.

[30] T.L. Hill, A. Cammarano, S.A. Neild and D.J. Wagg, An Analytical Method for the Optimisation of Weakly Nonlinear Systems, *Proceedings of the 9th International Conference on Structural Dynamics - EURODYN 2014*, Porto, Portugal, 2014.

[31] T.L. Hill, A. Cammarano, S.A. Neild and D.J. Wagg, Interpreting the Forced Response of a Two-Degree-Of-Freedom Nonlinear Oscillator using Backbone Curves, *Submitted to Journal of Sound and Vibration*, 2014.

[32] Y.S. Lee, G. Kerschen, A.F. Vakakis, P. Panagopoulos, L.A. Bergman, D.M. McFarland, Complicated Dynamics of a Linear Oscillator with an Essentially Nonlinear Local Attachment, *Physica D*, vol. 204, pp. 41-69, 2005.

[33] S.M. Roberts and J.S. Shipman, *Two-Point Boundary Value Problems: Shooting Methods*, New York, American Elsevier, 1972.

[34] M.W. Sracic and M.S. Allen, Numerical Continuation of Periodic Orbits for Harmonically Forced Nonlinear Systems, *Proceedings of the 29th International Modal Analysis Conference (IMAC XXIX)*, Jacksonville, Florida, 2011.

[35] R.J. Kuether and M.S. Allen, Computing Nonlinear Normal Modes using Numerical Continuation and Force Appropriation, *Proceedings of the ASME 2012 International Design Engineering Technical Conferences IDETC/CIE*, Chicago, Illinois, 2012.

[36] M. Geradin, D. Rixen, *Mechanical Vibrations; Theory and Application to Structural Dynamics*, Wiley, 1997.

[37] A.V. Kuznetsov, *Elements of Applied Bifurcation Theory*, Springer, New York, 2004.

[38] R.J. Kuether, L. Renson, T. Detroux, C. Grappasonni, G. Kerschen, M.S. Allen, Nonlinear Normal Modes, Modal Interactions and Isolated Resonance Curves, *Journal of Sound and Vibration*, in review.

[39] T. Detroux, L. Renson, and G. Kerschen, The Harmonic Balance Method for Advanced Analysis and Design of Nonlinear Mechanical Systems. In G. Kerschen, Ed., *Nonlinear Dynamics*, Volume 2, pp. 19-34, Springer International Publishing, 2014.